Binding energies of interstellar molecules on crystalline and amorphous models of water ice by ab initio calculations

Binding energies of interstellar molecules on water ice: ab-initio calculations

Stefano Ferrero,[1,2,#] Lorenzo Zamirri,[1,2] Cecilia Ceccarelli,[3] Albert Rimola,[4] and Piero Ugliengo.[*,1,2]

[1] Dipartimento di Chimica, Università degli Studi di Torino, via P. Giuria 7, 10125, Torino, Italy.

[2] Nanostructured Interfaces and Surfaces (NIS) Centre, Università degli Studi di Torino, via P. Giuria 7, 10125, Torino, Italy.

[3] Univiversité Grenoble-Alpes, CNRS, Institut de Planétologie et d'Astrophysique de Grenoble (IPAG), rue de la Piscine 414, 380008 Grenoble, France.

[4] Departament de Química, Universitat Autònoma de Barcelona, 08193 Bellaterra, Catalonia, Spain.

[#] Current address: Departament de Química, Universitat Autònoma de Barcelona, 08193 Bellaterra, Catalonia, Spain.

[*] Corresponding author: piero.ugliengo@unito.it

Abstract

In the denser regions of the interstellar medium (ISM), several molecules have been observed in the gas phase through their rotational transitions in the radio to far infrared wavelengths. In addition, near infrared observations have revealed the presence of sub-micron sized dust grains that, in the very cold (≤20 K) ISM regions, are covered by several layers of H_2O-dominated ices, "dirtied" by the presence of other volatile species. Calculating the binding energies (BEs) of the ISM molecules to ice surfaces is of extreme importance because they are key parameters for the astrochemical models that aim to reproduce the observed evolution of the ISM chemistry. In general, BEs can be inferred either from experimental techniques or by theoretical computations. In this work, we present a reliable computational methodology to evaluate the BE values of a large set (21) of astrochemically-relevant molecules, including radical species (4 cases). To this end, we consider different surface models mimicking the interstellar water ice mantles. The adopted models are periodically extended, either of crystalline and amorphous nature. Density functional theory (DFT), adopting the widely used B3LYP-D3 and M06-2X functionals, was used for predicting the species structure and BE. We found that each molecule does not have a single BE value but, on the contrary, multiple values, which depend on the molecule structure and its position on the ice. Finally, we compare the computed data with literature data, astrochemical databases and experimental works results and provide recommendations for the astrochemical modelers.

Keywords: icy dust grains, complex organic molecules, dense molecular clouds, interstellar medium, *ab initio*, DFT, surface modelling, .

1 Introduction

The presence of molecules under the extreme physical conditions of the interstellar medium (ISM) has been inconceivable by astronomers for a long period of time until the first diatomic species, namely CN, CH and CH^+, were detected in the ISM from optical and ultraviolet transitions (Douglas & Herzberg 1942; McKellar 1940; Swings & Rosenfeld 1937). Nowadays more than 200 molecular species (including radicals and ions) have been identified in the gas phase of diffuse and dense regions of the ISM (e.g. McGuire 2018).

The term "interstellar molecules" not only denotes proper molecular species but also cationic or anionic molecular species. They are usually observed in dense and diffuse molecular clouds, star forming regions and envelopes of dying stars. In general, interstellar matter is made of gas and sub-micrometer-sized dust grain particles. As inferred from near infrared (NIR) observations, the core of these grains consists of refractory materials, mainly silicates and carbonaceous materials based (e.g. Jones et al. 2013, 2017) The surface of these grains is usually covered by ice mantles, formed either by the adsorption of species from the gas phase or by chemical reactions occurring at the grain surface. The most abundant species of the ice mantles is H_2O, formed by the hydrogenation of O, O_2 and O_3 on the grain surfaces (e.g. Hiraoka et al. 1998; Dulieu et al. 2010; Oba et al. 2012). The water-rich ice is recognized from two specific NIR bands at about 3 and 6 μm which are associated with its O-H stretching and H-O-H bending modes, respectively (e.g. see the review by Boogert et al. 2015). In addition, species like CO, CO_2, NH_3, CH_4, CH_3OH and H_2CO have also been identified as minor constituents of the ice mantles, which, for this reason, are sometimes referred to as "dirty ices"(Boogert et al. 2015). Furthermore, spectroscopic comparisons between interstellar observations and laboratory spectra of interstellar ice sample analogous, principally based on the O-H stretching feature, have shown that these covering ices should present an amorphous-like structure resembling that from amorphous solid water (ASW) (Oba et al. 2009; Oberg et al. 2008; Watanabe & Kouchi 2008).

Ice surfaces are known to have an important role in the interstellar chemistry because they can serve as catalysts for chemical reactions which cannot proceed in the gas phase, such as the formation of H_2, the most abundant molecule in ISM ((Hollenbach & Salpeter 1971). Ice surfaces can catalyze reactions either by behaving as: i) passive third body, this way absorbing part of the excess of energy released in the surface processes (adsorption and/or chemical reaction); ii)

chemical catalyst, this way directly participating in the reaction reducing the activation energies; and iii) reactant concentrator, this way retaining the reactants and keeping them in close proximity for subsequent reaction (e.g., CO adsorption and retention for subsequent hydrogenation to form H_2CO and CH_3OH (e.g. Watanabe & Kouchi 2002 ; Rimola et al. 2014; Zamirri et al. 2019b). Molecular species formed on the grain surfaces can be later transferred to the gas phase by various desorption processes, most of which depend on the binding energies (BE) of the iced molecules (see below)

The chemical processes occurring in the ISM, both in the gas and in the solid phases, are usually simulated with numerical astrochemical models which aim to reproduce the evolution of the abundances of the mixture of chemical species under ISM conditions. Models that have large reaction networks are usually based on the rate equation approach (Herbst 2014), where the time evolution of the abundances of the astrochemical species is described by a set of coupled differential equations (e.g. Brown & Charnley 1990; Hasegawa et al. 1992; Hasegawa & Herbst 1993). One major drawback of the gas-grain models is that they cannot deal precisely with the stochastic nature of diffusive surface processes. For this reason, models based on Monte Carlo techniques have also been developed in order to overcome the issue (Tielens & Hagen 1992; Charnley et al. 1992; Lipshtat & Biham 2003; Chang & Herbst 2014). Additionally, more advanced models that can include processes arising from the multilayered nature of the ASW mantles have been developed too (Taquet et al. 2012, 2013; Lu, Chang & Aikawa 2018). However, the results of all these models are highly dependent on the values assumed for the BE on the ASW of the various species (e.g. Penteado et al. 2017).

Experimentally, the BEs of astrochemical species are measured by temperature programmed desorption (TPD) experiments. These experiments measure the energy required to desorb a particular species from the substrate, namely a desorption enthalpy, which is equal to the BE only if there are no activated processes (He et al. 2016) and if thermal effects are neglected. A typical TPD experiment consists of two phases. In the first one, the substrate, maintained at a constant temperature, is exposed to the species that have to be adsorbed coming from the gas phase. In the second phase, the temperature is increased until desorption of the adsorbed species–collected and analyzed by a mass spectrometer–occurs. The BE is then usually extracted by applying the direct inversion method on the Polanyi-Wigner equation (e.g. Dohnálek et al. 2001; Noble et al. 2012). The BE values obtained in this way strongly depend on the chemical composition and morphology of the substrate and also on whether the experiment is conducted in the monolayer or multilayer regime (e.g. Noble et al. 2012; Chaabouni et al. 2018; He et al. 2016). Another issue related to the

TPD technique is that it cannot provide accurate BEs for radical species as they are very reactive. In literature, there are many works that have investigated the desorption processes by means of the TPD technique (e.g. Collings et al. 2004; Dulieu et al. 2013; Fayolle et al. 2015; He et al. 2016; Noble et al. 2012; Smith et al. 2016) but they have been conducted for just a handful of important astrochemical species, whereas a typical network of an astrochemical model can contain up to five hundred species and very different substrates. In a recent work, Penteado et al. (2017) collected the results of these experimental works, trying to be as homogeneous as possible in terms of different substrates, estimating the missing BE values from the available data and performing a systematic analysis on the effect that the BE uncertainties can have on astrochemical model simulations.

BE values can also be obtained by means of computational approaches which, in some situations, can overcome the experimental limitations. Many computational works have so far focused on a few important astrochemical species like H, H_2, N, O, CO, CO_2, in which BEs are calculated on periodic/cluster models of crystalline/amorphous structural states using different computational techniques (Al-Halabi & Van Dishoeck 2007; Ásgeirsson et al. 2017; Karssemeijer et al. 2014b, 2014a; Senevirathne et al. 2017; Shimonishi et al. 2018; Zamirri et al. 2019a). In addition, other works have computed BE in a larger number of species but with a very approximate model of the substrate. For example, in a recent work by Wakelam et al. (2017) BE values of more than 100 species are calculated by approximating the ASW surface with a single water molecule. The authors then fitted the most reliable BE measurements (16 cases) against the corresponding computed ones, obtaining a good correlation between the two data sets. In this way, all the errors in the computational methods and limitations due to the adoption of a single water molecule are compensated by the fitting with the experimental values, in the view of the authors. The resulting parameters are then used to scale all the remaining computed BE to improve their accuracy. This clever procedure does, however, consider the proposed scaling universal, leaving aside the complexity of the real ice surface and the specific features of the various adsorbates. In a similar work, Das et al. (Das 2018) have calculated the BEs of 100 species by increasing the size of a water cluster from one to six molecules, noticing that the calculated BE approaches the experimental value when the cluster size is increased. As we will show in the present work, these approaches, relying on an arbitrary and very limited number of water molecules, cannot, however, mimic a surface of icy grain. Furthermore, the strength of interaction between icy water molecules as well as with respect to the adsorbates depends on the hydrogen bond cooperativity, which is underestimated in small water clusters.

In this work, we followed a different approach, focusing on extended periodic ice models, either crystalline or amorphous, adopting a robust computational methodology based on a quantum mechanical approach. We simulate the adsorption of a set of 17 interstellar relevant molecules and 4 radical species on several specific exposed sites of the water surfaces of both extended models. BE values have been calculated for more than one binding site (if present) to provide some statistical representativeness. Different approaches, with different computational cost, have been tested and compared, and the final computed BEs have been compared with data from the computational approaches of Wakelam et al, Das et al and data from UMIST and KIDA databases as well as available experimental data (Das 2018; McElroy et al. 2013; Wakelam et al. 2017, 2015). One added value of this work is the definition of both a reliable, computationally cost-effective *ab-initio* procedure designed to arrive to accurate BE values and an ice grain atomistic model, that can be applied to predict BE of any species of astrochemical interest.

2 Computational Details

2.1 Periodic simulations

Water ice surfaces have been modelled enforcing periodic boundary conditions to define icy slabs of finite thickness either entirely crystalline or of amorphous nature. Adsorption is then carried out from the void region above the defined slabs. Periodic calculations have been performed with the *ab initio* CRYSTAL17 code.(Dovesi et al. 2018a) This software implements both the Hartree-Fock (HF) and Kohn-Sham self-consistent fields methods for the solution of the electronic Schrödinger equation, fully exploiting, if present, the crystalline/molecular symmetry of the system under investigation. CRYSTAL17 adopts localized Gaussian functions as basis sets, similar to the approach followed by molecular codes. This allows CRYSTAL17 to perform geometry optimizations and vibrational properties of both periodic (polymer, surfaces and crystals) and non-periodic (molecules) systems with the same level of accuracy. Furthermore, the definition of the surfaces through the slab model allows to avoid the 3D fake replica of the slab as forced when adopting plane waves basis set.

Computational parameters are set to values ensuring good accuracy in the results. The threshold parameters for the evaluation of the Coulomb and exchange bi-electronic integrals (TOLINTEG keyword in the code(Dovesi et al. 2018a)) have been set equal to 7, 7, 7, 7, 14. The needed density functional integration are carried out numerically over a grid of points, which is based on an atomic partition method developed by Becke.(Becke 1988) The standard pruned grid

(XLGRID keyword in the code(Dovesi et al. 2018a)), composed by 75 radial points and a maximum of 974 angular points, was used. The sampling of the reciprocal space was conducted with a Pack-Monkhorst mesh,(Pack & Monkhorst 1977) with a shrinking factor (SHRINK in the code(Dovesi et al. 2018a)) of 2, which generates 4 *k* points in the first Brillouin zone. The choice of the numerical values we assigned to these three computational parameters is fully justified in the Supporting Information (SI).

Geometry optimizations have been carried out using the Broyden-Fletcher-Goldfarb-Shanno (BFGS) algorithm,(Broyden 1970; Fletcher 1970; Goldfarb 1970; Shanno 1970) relaxing both the atomic positions and the cell parameters. We adopted the default values for the parameters controlling the convergence were maintained, i.e., difference in energy between two subsequent steps, 10^{-7} Hartree; and maximum components and root-mean-square of the components of the gradients and atomic displacements vectors, 4.5×10^{-4} Hartree Bohr^{-1} and 3.0×10^{-4} Hartree Bohr^{-1}, and 1.8×10^{-3} Bohr and 1.2×10^{-3} Bohr, respectively.

All periodic calculations were grounded on either the density functional theory (DFT) or the HF-3 corrections (HF-3c) method(Hohenberg & Kohn 1964; Sure & Grimme 2013). Within the DFT framework, different functionals were used to describe closed- and open-shell systems. For the former, we used the hybrid B3LYP method,(Becke 1993; Lee et al. 1988) which has been shown to provide a good level of accuracy for the interaction energies of non-covalent bound dimers,(Kraus & Frank 2018) added with the D3-BJ correction for the description of dispersive interactions.(Grimme et al. 2011, 2010) For open-shell systems, treated with a spin-unrestricted formalism,(Pople et al. 1995) we used the hybrid M06-2X functional, which has been proved to give accurate results in estimating the interaction energy of non-covalent binary complexes involving a radical species and a polar molecule.(Tentscher & Arey 2013) The choice of this two different functionals is justified by two previous works describing the accuracy on the energetic properties of molecular adducts.(Kraus & Frank 2018; Tentscher & Arey 2013) For all periodic DFT calculations we used the Ahlrichs' triple-zeta quality VTZ basis set, supplemented with a double set of polarization functions.(Schäfer et al. 1992) In the following, we will refer to this basis set as "A-VTZ*" (see **Table S4** in the SI for details of the adopted basis set).

The HF-3c method is a new method combining the Hartree-Fock Hamiltonian with the minimal basis set MINI-1(Tatewaki & Huzinaga 1980) and with three *a posteriori* corrections, respectively for: i) the basis set superposition error BSSE (error arising when Gaussian functions are used) (Jansen & Ros 1969)·(Liu & Mclean 1973)); ii) the dispersive interactions; iii) short-ranged deficiencies due to the adopted minimal basis set.(Sure & Grimme 2013)

Harmonic frequency calculations were carried out on the optimized geometries to characterize the stationary points of each structure. Vibrational frequencies have been calculated at the Γ point by diagonalizing the mass-weighted Hessian matrix of second order energy derivatives with respect to atomic displacements.(Pascale et al. 2004; Zicovich-Wilson et al. 2004) To avoid computational burden, only a portion of the systems have been considered in the construction of the Hessian matrix, including the adsorbed species and the spatially closest interacting water molecules of the ice surface. This "fragment" strategy for the frequency calculation has already been tested by some of us in previous works and is fully justified by the non-covalent nature of the interacting systems where the coupling between the vibrational modes of bulk ice and adsorbate moieties is negligible.(Rimola et al. 2008; Tosoni et al. 2005; Zamirri et al. 2017) The Hessian matrix elements have been evaluated numerically by a six-points formula (NUMDERIV=2 in the code(Dovesi et al. 2018b)), based on two displacements of ±0.001 Å for each nuclear cartesian coordinates from the minimum structure.

2.2 BE calculation and Counterpoise correction

When Gaussian basis sets are used, a spurious contribution arises in the calculation of the molecule/surface interactions, called BSSE (basis set superposition error).(Boys & Bernardi 1970) In this work, the BSSE for DFT calculations has been corrected making use of the *a posteriori* Counterpoise correction (CP) by Boys and Bernardi.(Davidson & Feller 1986) The CP-corrected interaction (ΔE^{CP}) energy has been calculated as

$$\Delta E^{CP} = \Delta E^{*} + \delta E + \Delta E_{L} - BSSE \qquad \mathbf{1}$$

Where ΔE^{*} is the deformation free interaction energy, δE is the total contribution to the deformation energy, and ΔE_{L} is the lateral interaction (adsorbate-adsorbate interaction) energy contribution. Details of the calculation of each energetic term of Equation **1** can be found in the SI.

By definition, BE is the opposite of the CP-corrected interaction energy:

$$\Delta E^{CP} = -BE \qquad \mathbf{2}$$

In the following we will label as BE *disp* the pure dispersion contribution to the BE due to the D3 contribution to the energy. The remaining contribution to BE, due to the electrostatic, polarization and charge transfer effects will be referred as "electrostatic" contribution for easiness of notation.

2.3 BE refinement with the embedded cluster method

With the aim of refine the periodic DFT BE values for the crystalline ice model, single point energy calculations have been carried out on small clusters, cut out from the crystalline ice model, using a higher level of theory than the DFT methods with the Gaussian09 program. The adopted cluster models were derived from the periodic systems and are described in the dedicated subsection of the "Results and Discussion section" (see below). These refinements have been performed through the ONIOM2 approach,(Dapprich et al. 1999) dividing the systems in two parts that are described by two different levels of theory. The *model system* (i.e., a small moiety of the whole system including the adsorbate and the closest water molecules) was described by the *high* level of theory represented by the single- and double-electronic excitations coupled-cluster method added with a perturbative description of triple excitations (CCSD(T)) with the Jun-cc-pVTZ basis set.(Bartlett & Musiał 2007; Papajak et al. 2011) The *real system* (*i.e.*, the whole system) was described by the DFT level of theory adopted in the periodic calculations with the two different functionals for open- and closed-shell species. In the ONIOM2 methodology, the BE can be written as:

$$\mathrm{BE(ONIOM2)} = BE(Low, Real) + \Delta BE$$
$$\Delta BE = \mathrm{BE}(High, Model) - \mathrm{BE}(Low, Model) \qquad \textbf{3}$$

Our choices about the model and real systems will be extensively justified in the dedicated subsection of the "Results and Discussion" section.

3 Results and Discussion

3.1 Ice surface models

3.1.1 Crystalline model

Despite the amorphous and perhaps porous nature of the interstellar ice, we adopted, as a paradigmatic case, a proton-ordered crystalline bulk ice model usually known as *P-ice*(Casassa et al. 1997) (*$Pna2_1$* space group). From P-ice bulk, we cut out a *slab model*, i.e. a 2D-periodic model representing a surface. Consequently, periodic boundary conditions are maintained only along the two directions defining the slab plane, while the third direction (z-axis) is non-periodic and defines the slab thickness. The slab model adopted in this work represents the P-ice (010) surface, in accordance with previous work.(Zamirri et al. 2018) This slab consists of twelve atomic layers, is stoichiometric and has a null electric dipole moment across the z-axis. This ensure an electronic stability of the model with the increase of the slab thickness.(Tasker 1979) The slab structure has

been fully optimized (unit cell and atomic fractional coordinates) at both B3LYP-D3/A-VTZ* and M06-2X/A-VTZ* DFT levels. As it can be seen from **Figure 1A**, the (010) P-ice unit cell is rather small, showing only one dangling hydrogen (dH) and oxygen (dO) as binding sites. To increase the number of adsorption sites and minimize the lateral interactions among replicas of the adsorbate we also considered a 2x1 supercell. The electrostatic potential maps (EPMs, see **Figure 1B** and **C**), clearly reveal the dH sites (blue positive EPM regions) of the surface and the dO sites (red, negative EPM regions).

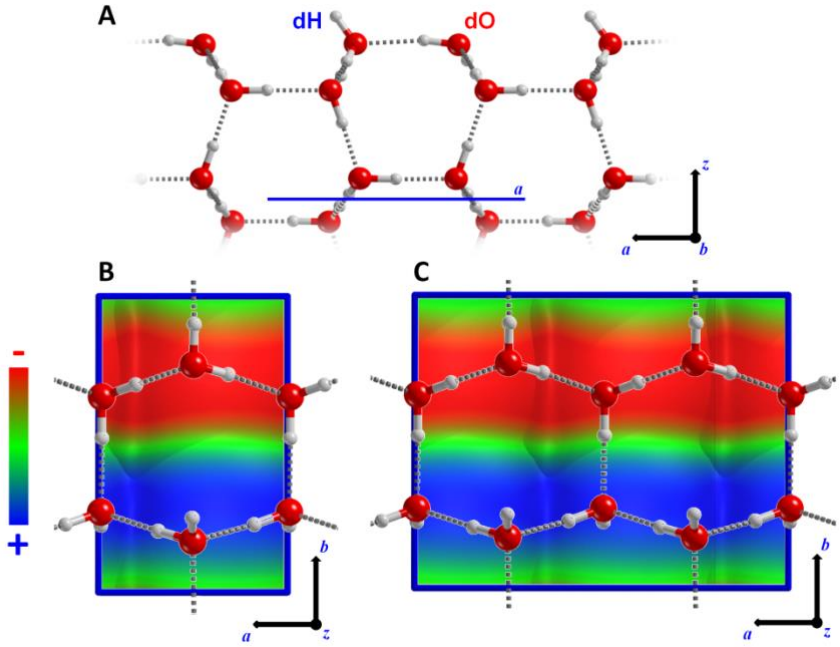

Figure 1. (010) slab model of P-ice. A) Side view of along the ***b*** lattice vector. B) Top view of the 1x1 unit cell (|***a***| = 4.500 Å and |***b***| = 7.078 Å) superimposed to the electrostatic potential map, EPM. C) Top view of the 2x1 supercell (|***a***| = 8.980 Å, |***b***| = 7.081 Å) superimposed to the EPM. The ISO value for the electron density where the EP is mapped is set equal to 10^{-6} au. Colour code: +0.02 au (blue, positive), 0.00 au (green, neutral) and -0.02 au (red, negative).

3.1.2 Amorphous model

As anticipated, the (010) P-ice surface might not be a physically sound model to represent actual interstellar ice surfaces, due to the evidence, from the spectroscopic feature of the interstellar ice, of its amorphous nature (Boogert et al. 2015). The building up of amorphous surface models is a non-trivial and not unique procedure, because of the lack of a consistent and universally-accepted strategy. One common approach is to start from a crystalline model and heat it up to relatively high temperature by running molecular dynamics simulations (MDs) for few picoseconds. This step is followed by thermal annealing to freeze the ice in a glassy amorphous state. In this work, we adopted a different strategy. We refer to a recent work by Shimonishi *et al.*(Shimonishi et al. 2018) in which the BEs of a set of atomic species was computed on several water clusters, previously

annealed with MD simulations. We re-optimized (at B3LYP-D3/A-VTZ* level only) the whole set of ice clusters and the three most stable clusters, composed by 20 water molecules each, were merged together to define a unit cell of an amorphous periodic ice. This procedure mimics somehow the collision of nanometric scale icy grains occurring in the molecular clouds. The merge of the three clusters was carried out by matching the dHs regions of one cluster with the dOs ones of the other. As a result, we ended up with a large 3D-periodic unit cell (with lattice parameters $|\boldsymbol{a}|$ = 20.11 Å, $|\boldsymbol{b}|$ = 11.8 Å and $|\boldsymbol{c}|$ = 11.6 Å) envisaging 60 water molecules. This initial bulk model was optimized at HF-3c level in order to fully relax the structure from the internal tensions of the initial guess. After this step, we cut out a 2D-periodic slab from the bulk structure. The amorphous slab is composed by 60 water molecules in the unit cell, and was further fully optimized (unit cell size and atomic coordinates) at the HF-3c level, B3LYP-D3/A-VTZ* and M06-2X/A-VTZ* levels of theory. The three final structures show little differences in the positions of specific water molecules and, on the whole, the structures are very similar (**Figure 2**). The computed electric dipole moment across the non-periodic direction (1.7, 0.7 and 0.3 Debyes for the HF-3c, B3LYP-D3 and M06-2X structures, respectively) showed a very good agreement between different models.

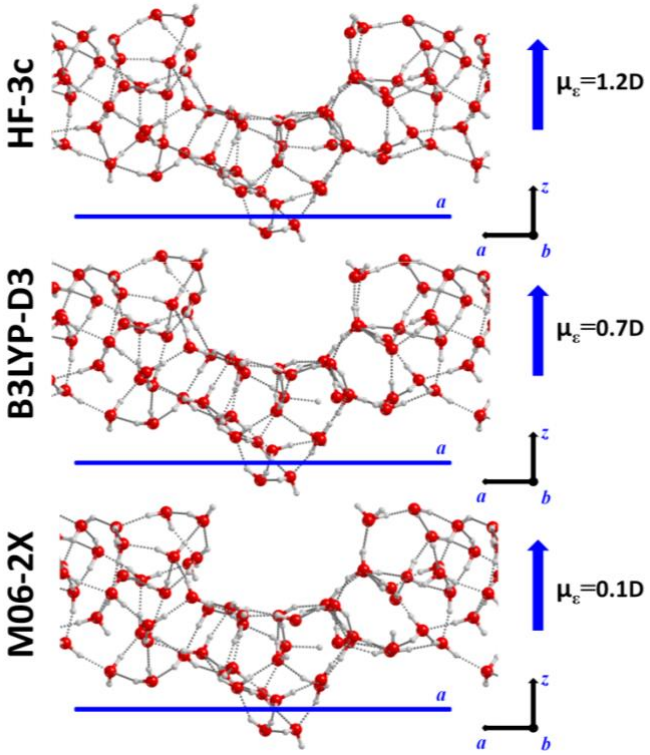

Figure 2 Side view of the amorphous slab models. The cell parameter ***a*** is highlighted as a blue line. Electric dipole moments ($\boldsymbol{\mu}_\varepsilon$) along the **z** direction shown on the right side.

These amorphous slab models show different structural features for the upper and lower surfaces which imparts the residual dipole moment across the slab, and, consequently, exhibit a variety of different binding sites for adsorbates. To characterize the electrostatic features of these

sites, we resorted to the EPMs for the top/bottom surfaces of each optimized slab (**Figure 3**). The general characteristics are very similar for the three models: B3LYP-D3 and M06-2X giving the closest maps. HF-3c tends to enhance the differences between positive/negative regions due to overpolarization of the electron density due to the minimal basis set. "Top" surfaces show a hydrophobic cavity (the central greenish region, Figure 3), absent in the P-ice slab, surrounded by dHs positive spots. "Bottom" surfaces shows several prominent negative regions (from five dOs) mixed with less prominent positive potentials (due to four buried dHs).

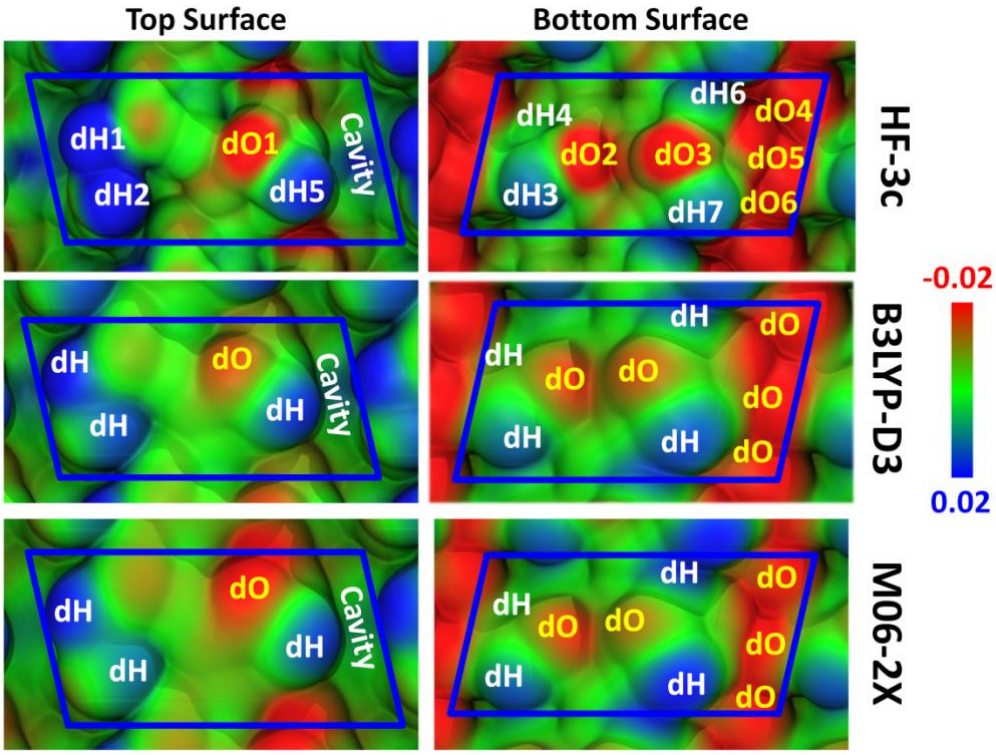

Figure 3 Colour-coded electrostatic potential energy maps (EPMs) mapped to the electron density for the "top" and "bottom" surfaces of the amorphous slab (HF-3c, B3LYP-D3 and M06-2X optimized geometries). dO and dH sites are also labelled. The ISO value for the electron density is set equal to 10^{-6} au to which the EP is mapped out. EPM color code: +0.02 au (blue, positive), 0.00 au (green, neutral) and -0.02 au (red, negative).

3.2 BEs on crystalline ice

In this work, we simulated the adsorption of 17 closed-shell species and 4 radicals, shown in **Figure 4**. For each structure, geometry optimizations of the molecule/surface adducts (unit cell plus all atomic coordinates without constraints) were performed: initial structures were guessed by manually setting the maximum number of H-bonds between the two partners. The pure role of dispersion is estimated by extracting the D3 contribution from the total energy at B3LYP-D3 level of theory. The energetics of the adsorption processes were then computed according to Equation **1**,

and the results shown in **Table 1**, whereas all the optimized geometries alongside other interesting energetic features are reported in the SI.

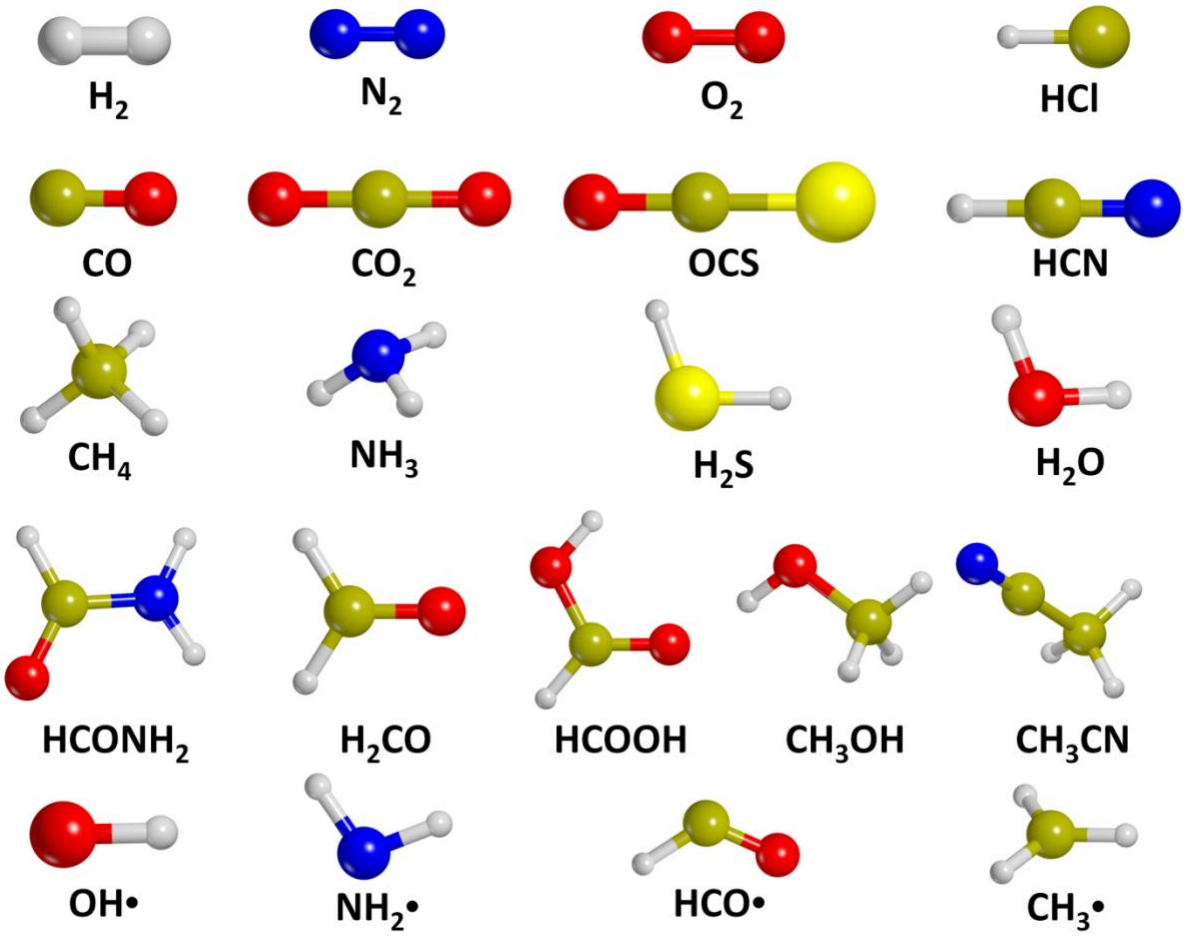

Figure 4 Set of molecular and radical species adopted within this work for the calculation of binding energy on different ice models. O_2 is an open-shell (spin-triplet) species.(Borden et al. 2017)

As it can be seen from the results of **Table 1**, a range of interactions of different strength are established between the adsorbed species and the crystalline P-ice surface. Some molecules do not possess a net electric dipole moment, while exhibiting relevant electric quadrupole moments (i.e., H_2, N_2 and O_2) or multipoles moments of higher order (i.e., CH_4, see their EPMs in **Figures S1-S4**). For these cases, only weak interactions are established so that BE are lower than 15 kJ mol^{-1} (see BE *disp* values in Table 1). Interestingly, for the N_2, O_2 and CH_4 cases, interactions are almost repulsive if dispersive contributions are not accounted for in the total BE (compare BE *disp* with BE *no disp* values of **Table 1**). Therefore, the adsorption is dictated by dispersive forces, which counterbalance the repulsive electrostatic interactions. For the H_2 case, electrostatic interactions are

attractive mainly because of the synergic effect of both the surface dH and the dO on the negative and positive parts of the H_2 quadrupole, respectively (see **Figure S1**).

CO, OCS and CO_2 also exhibit a quadrupole moment, but due to the presence of heteroatoms in the structure, they can also establish H-bonds with the dH site. Consequently, BEs are larger than the previous set of molecules (i.e., > 20 kJ mol^{-1}, see **Table 1**). For these three cases, pure electrostatic interactions are attractive, but the dispersion contribution is the most dominant one over the total BE values (compare BE *disp* and BE *no disp* values of **Table 1**). CO, in addition to a net quadrupole, also possesses a weak electric dipole, with the negative end at the carbon atom (see its EPM in **Figure S5**).(Zamirri et al. 2017) Thus, although the two negative poles (C and O atoms) of the quadrupole can both interact with the positive dH site, the interaction involving the C atom is energetically slightly favoured over the O atom.(Zamirri et al. 2017, 2019a) Accordingly, we only considered the C-down case, the computed BE being in good agreement with previous works.(Zamirri et al. 2018, 2017) OCS also possesses a dipole and can interact with the surface through either its S- or O-ends, through dO or dH sites. However, due to the softer basic character of S compared to O, the interaction through oxygen is preferred and only considered here.

NH_3, H_2O, HCl, HCN and H_2S are all amphiprotic molecules that can both serve as acceptors and donors of H-bonds from/to the dH and dO sites. The relative strong H-bonds with the surface result in total BE values that are almost as twice as higher than the values of the previous set of molecules (i.e., CO, OCS and COS). Although also in these cases dispersive forces play an important contribution to the BE, the dominant role is dictated by the H-bonding contribution.

For the adsorption of CH_3OH, CH_3CN and the three carbonyl-containing compounds, i.e., H_2CO, $HCONH_2$ and HCOOH, all characterized by large molecular sizes, we adopted the 2x1 supercell (shown in **Figure 1**) to minimize the lateral interactions between adsorbates. Consequently, two dHs and two dOs are available for adsorption. Therefore, for some of these species (i.e., the carbonyl-containing ones), we started from more than one initial geometry to improve a better sampling of the adsorption features on the (010) P-ice surface (the different cases on the supercell are labeled SC1 and SC2 in **Table 1**and the geometries are reported in **Figures S13-S21**). The BE values of these species are among the highest ones, due to the formation of multiple H-bonds with the slab (and therefore increasing the electrostatic contribution to the interactions), and a large dispersion contributions due to the larger sizes of these molecules with respect to the other species.

The adsorption study has also been extended to four radicals (i.e., OH• NH_2• CH_3• HCO•), since they are of high interest due to their role in the formation of interstellar compounds.(Bennett

& Kaiser 2007; Sorrell 2002) OH• and NH_2• form strong H-bonds with the dH and dO sites of the slab, at variance with CH_3• and HCO• cases, as shown by the higher BE values. Because of the nature of the M06-2X functional, we cannot separate the dispersion contributions to the total BEs. Interestingly, in all cases, we did not detect transfer of the electron spin density from the radicals to the ice surface, i.e., the unpaired electron remains localized on the radical species upon adsorption.

3.3 ONIOM2 correction

As described in the Computational Details section, the ONIOM2 methodology has been employed to check the accuracy of the B3LYP-D3/A-VTZ* and M06-2X/A-VTZ* theory levels, both representing the *Low* level of calculation. For this specific case to reduce the computational burden, we only considered 15 species, leaving aside N_2, O_2, H_2O, CH_4, CH_3CN and ·CH_3 radical. Here, the *Real system* is the periodic P-ice slab model without adsorbed species. Therefore, the $\mathrm{BE}(Low, Real)$ term in Equation **3** corresponds to the BEs at the DFT theory levels, hereafter referred to as $\mathrm{BE}(DFT, ice)$. The *model system* is carved from the optimized geometry of the periodic system: it is composed by the adsorbed molecule plus n ($n = 2, 6$; the latter only for the H_2 case) closest water molecules of the ice surface to the adsorbates (see **Figure S2** of the SI). For the model systems, two single point energy calculations have been carried out: one at the *high* level of theory, i.e., CCSD(T) with a June-cc-pVTZ basis set (shortly referred to as TZ), calculated with Gaussian09, and the other at the *low* level of theory, employing the same DFT methods as in the periodic calculations, calculated with CRYSTAL17. For the sake of clarity, we renamed the two terms $\mathrm{BE}(High, Model)$ and $\mathrm{BE}(Low, Model)$ in Equation **3** for any molecular species μ, as $\mathrm{BE}(\mathrm{CCSD(T)}, \mu - n\mathrm{H_2O})$ and $\mathrm{BE}(\mathrm{DFT}, \mu - n\mathrm{H_2O})$, respectively.

As CCSD(T) is a wavefunction-based methods, the associated energy strongly depend on the quality of the adopted basis set.(Cramer 2004) Consequently, accurate results are achieved only when complete basis set extrapolation is carried out,(Cramer 2004); accordingly, we adopted correlation consistent basis sets,(Dunning Jr 1989) here named as cc-pV*N*Z, where "cc" stands for correlation consistent and "*N*" stands for double (D), triple (T), quadruple (Q), etc... Therefore, we performed different calculations improving the quality of the basis set from June-cc-pVDZ to June-cc-pVQZ (and even June-cc-pV5Z when feasible) extrapolating the $\mathrm{BE}(\mathrm{CCSD(T)}, \mu - n\mathrm{H_2O})$ values for $N \to \infty$. **Figure 5** shows, using NH_3 as illustrative example, the plot of the $\mathrm{BE}(\mathrm{CCSD(T)}, \mu - n\mathrm{H_2O})$ values as a function of $1/L^3$, where L is the cardinal number corresponding to the *N* value for each correlation-consistent basis set. For all other species, we observed similar trends. This procedure was used in the past to extrapolate the BE value of CO adsorbed at the Mg(001) surface.(Ugliengo & Damin 2002)

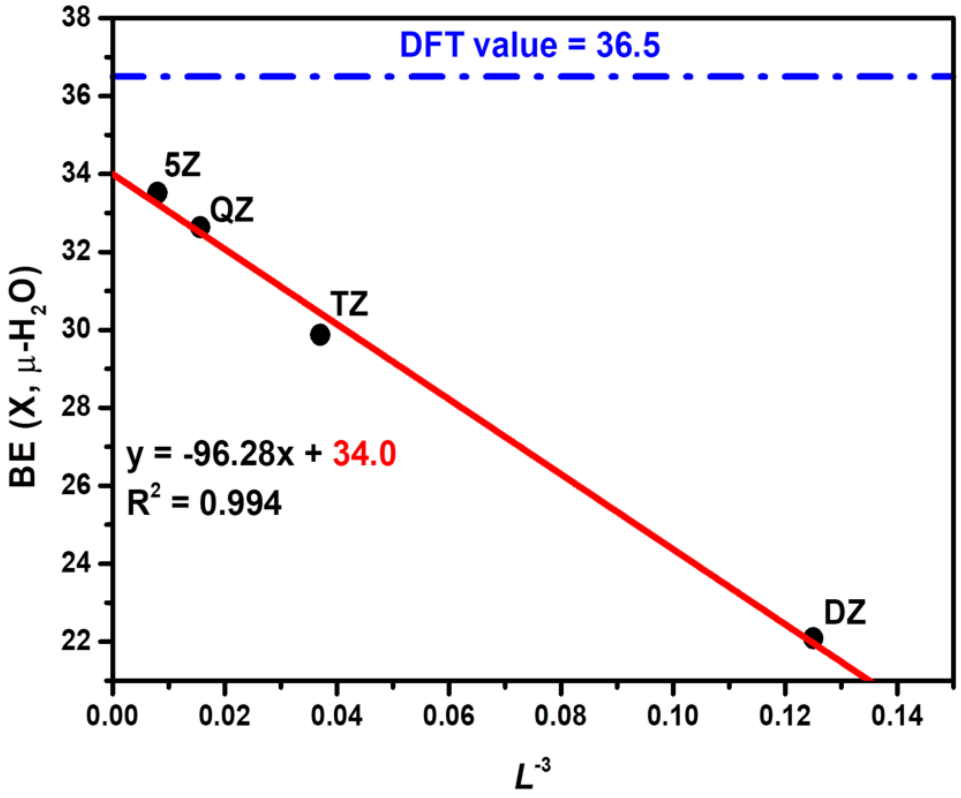

Figure 5 $\mathrm{BE(X}, \mu - n\mathrm{H_2O})$ extrapolated value at infinite basis set for the case of NH_3. The dashed-dot blue line represents the BE computed for the periodic system at DFT//A-VTZ* level (36.5 kJ mol^{-1}). Solid red line represents the linear fit of the $\mathrm{BE(X}, \mu - n\mathrm{H_2O})$ values (red squares) calculated with DZ, TZ, QZ and 5Z basis sets. The extrapolated $\mathrm{BE(CCSD(T)}, \mu - n\mathrm{H_2O})$ at infinite basis set is highlighted in red in the fitting equation (34.0 kJ mol^{-1}).

The procedure gives for the extrapolated $\mathrm{BE(CCSD(T)}, \mu - n\mathrm{H_2O})$ a value of 34.0 kJ mol^{-1} in excellent agreement with the value compute by the plain B3LYP-D3/A-VTZ* at periodic level of 36.5 kJ mol^{-1}(see **Figure 5**). Very similar agreement were computed for all considered species and we can confidently assume the periodic B3LYP-D3/A-VTZ* (closed shell molecules) or the M06-2X/A-VTZ* (radical species) plain results as reliable and accurate enough.

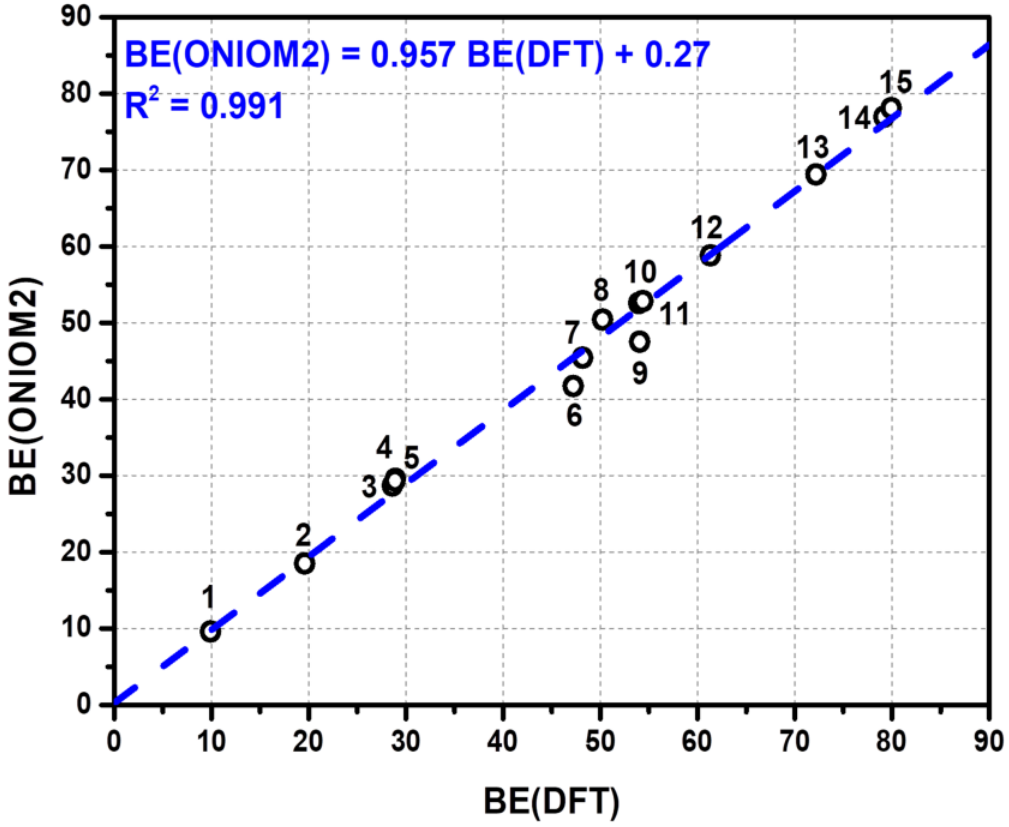

Figure 6 Linear fit between periodic DFT/A-VTZ* BE values (BE(DFT)) and the basis set extrapolated ONIOM2 BE values (BE(ONIOM2)). All values are in kJ mol^{-1}. Fit parameters are also reported. Legend: 1:H_2; 2:CO; 3:CO_2; 4:$HCO^{\bullet}$; 5:OCS; 6:H_2S; 7:HCN; 8:$NH_2^{\bullet}$; 9:H_2CO; 10:HCl; 11:$OH^{\bullet}$; 12:NH_3; 13:CH_3OH; 14:HCOOH; 15:$HCONH_2$;

3.4 Composite DFT//HF-3c method for the BE calculation on the (010) P-ice surface

In the previous Section we proved the DFT/A-VTZ* as a reliable and accurate methods adopted to compute the BEs of molecules and radicals on the crystalline (010) P-ice ice slab. However, even this approach can become very computational costly when adopting amorphous model of the interstellar ice as larger unit cells are needed to enforce the needed randomness in the water structure. Therefore, we tested the efficiency and accuracy of the cost-effective computational HF-3c method (see Computational section for details).

To this end, we adopted a composite procedure which has been recently assessed and extensively tested in the previous work of some of us on the structural and energetic features of molecular crystals, zeolites and biomolecules (Cutini et al. 2016a, 2019, 2016b). We started from the DFT/A-VTZ* optimized structure just discussed for the crystalline ice. We re-optimize each structure at HF-3c level to check the changes in the structures followed by a single point energy calculations at the two DFT/A-VTZ* levels from which the final BE is computed.

The results obtained are summarized in **Figure 7** in the form of a linear fit between BE values obtained at the full periodic DFT methods (BE(DFT//DFT)) against the composite DFT//HF-3c computational procedure (BE(DFT//HF-3c)).

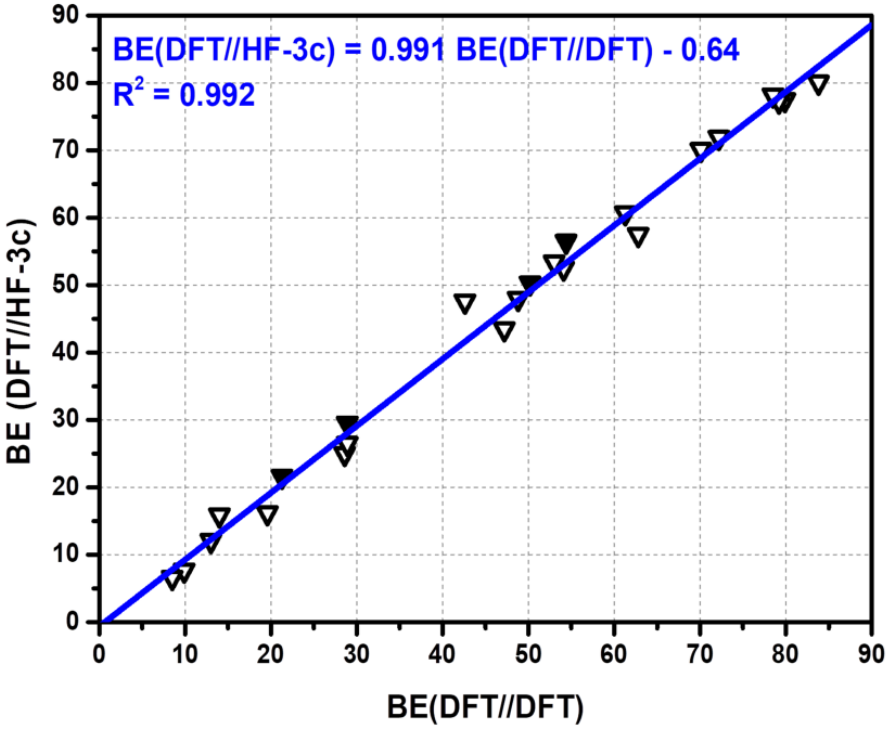

Figure 7 Linear fit between the BEs values calculated with the full DFT computational scheme and the BEs values calculated with the composite DFT//HF-3c computational scheme (all values in kJ mol^{-1}). Black-filled and empty triangles stand for open-shell and closed-shell species, respectively. Figure 6 e 7 can be fused in a) and b) horizontally

Results indicate that the composite BE(DFT//HF-3c) method matches very well the BE(DFT//DFT) values. The largest percentage differences are found for the smallest BEs, that is, those dominated by dispersion interactions or very weak quadrupolar interactions (i.e., N_2, O_2, H_2 and CH_4) in which the deficiencies of the minimal basis set encoded in the HF-3c cannot be entirely recovered by the internal corrections. For higher BE values, the match significantly improves, in some cases being almost perfect. Even for radicals, the composite approach gives good results. It is worth mentioning that HF-3c optimized geometries are very similar to the DFT-optimized ones (only slight geometry alterations occurred), indicating that the adducts are well-defined minima in both potential energy surfaces. In the following, we will adopt the composite method to study the adsorption of all 21 species on the proposed amorphous slab models, a computationally very expensive task at full DFT/A-VTZ* level.

Table 1 Resume of data obtained for the crystalline P-ice (010) slab with DFT//DFT and DFT//HF-3c methods. Legend: "BE *disp*":total B3LYP-D3 BE, "BE *no disp"*: DFT values without D3 correction*;"-disp (%)":*absolute (percentage) contribution of dispersive forces to the total BE *disp.*

Species	(010) P-ice crystalline slab DFT//DFT			(010) P-ice crystalline slab DFT//HF-3c		
	BE *disp*	**BE *no disp***	**-disp(%)**	**BE *disp***	**BE *no disp***	**-disp(%)**
H_2	9.9	4.7	5.2(53)	7.7	2.0	5.7(74)
O_2	8.5	-3.1	8.6(137)	6.6	-0.7	7.3(110)
N_2	13.0	-0.6	13.6(104)	12.1	-1.5	13.6(160)
CH_4	14.0	-1.9	15.9(113)	15.9	-2.9	18.8(118)
CO	19.6	5.8	13.8(71)	16.2	0.5	15.7(97)
CO_2	28.6	12.8	15.8(55)	25.0	7.8	17.2(69)
OCS	28.9	1.0	27.9(97)	26.5	2.2	24.3(92)
HCl	54.1	36.6	17.4(32)	52.5	29.0	18.6(39)
HCN	42.6	25.5	17.1(29)	47.6	27.2	25.3(48)
H_2O	70.1	56.9	13.2(19)	70.1	56.6	13.4(19)
H_2S	47.2	28.1	19.1(40)	43.5	26.6	17.5(40)
NH_3	61.3	46.0	15.4(25)	60.7	45.6	15.1(25)
CH_3CN	62.8	37.0	25.8(41)	57.5	27.1	21.6(44)
CH_3OH	72.2	50.0	22.2(31)	71.9	50.1	18.6(27)
H_2CO-SC1	48.8	32.3	16.5(34)	48.0	33.7	19.7(37)
H_2CO-SC2	53.0	30.7	22.3(42)	53.4	30.9	17.1(36)
$HCONH_2$-SC1	79.9	53.7	26.2(33)	77.5	51.2	26.3(34)
$HCONH_2$-SC2	83.8	53.9	30.0(36)	80.1	50.5	29.6(37)
HCOOH	79.2	60.9	18.2(23)	77.3	59.6	17.6(23)
HCOOH-SC	78.5	60.7	16.8(21)	78.2	62.7	15.5(20)
OH•	54.4*	-	-	56.5*	-	-
HCO•	28.9*	-	-	29.5*	-	-
CH_3•	21.3*	-	-	21.6*	-	-
NH_2•	50.2*	-	-	50.3*	-	-

* For radical species (energy at M06-2X level) we cannot discern between *disp* and *no disp* data

3.5 BEs on amorphous ice

On the amorphous slab model, due to the presence of different binding sites, a single BE value is not representative of the whole adsorption processes as it was the case for almost all adsorbates on the crystalline surface. Therefore, we computed the BE with the composite DFT//HF-3c procedure by sampling different adsorption sites at both the "top" and "bottom" surfaces of the amorphous slab. The starting initial structures of each adsorbate were set by hand, with the help of the EPMs (see Figure 3). For each molecule, at least four BE values have been computed on different surface sites. We reported in **Table 2**, the MIN, MAX and average values of the BE together with the estimated standard deviation. These values are compared with the ones computed for the crystalline ice, those from the recent work by Das et al (Das 2018), those corrected following the Wakelam's procedure (Wakelam et al. 2017) as well as the experimental set of data from UMIST (McElroy et al. 2013),the set of experimental/computed data from KIDA (Wakelam et al. 2015) databases and the available experimental data (see Table 2 for references). **Figure 8** reports a selection of the most representative cases with the comparison between crystalline and

amorphous binding energies. The amorphous nature of the ice can yield large differences in the calculated BEs with respect to the crystalline values. **Figure 8** shows that while binding energies for crystalline *vs* amorphous ices are very close to each other for H_2, O_2, N_2, CH_4, CO, CO_2, OCS, the ones computed for the remaining molecules for the crystalline ice fall in the highest range of the distribution of the amorphous BE values. This behavior can be explained considering the smaller distortion energy cost upon adsorption for the crystalline ice compared to the amorphous one. The different local environment provided by crystalline vs amorphous ices is also the reason for HCl being molecularly adsorbed at the crystalline ice while becomes dissociated at the amorphous one. Probably this difference in behavior will not occur for FH which is expected to be molecularly adsorbed on both ices due to its higher bond strength compare to HCl. Nevertheless, as we did not explore exhaustively all possible configurations of the adsorbates at the amorphous surfaces, we cannot exclude that some even more/less energetic binding cases remain to be discovered. Some adsorbates show similar trends in the BEs, despite their different chemical nature. This is shown in **Figure 9**, in which we plot the BE values for a set of molecules that have been adsorbed at the same adsorption sites. The BE distributions for the H_2CO and HCOOH are very similar (in their relative values), and those for CH_3OH and $HCONH_2$ show some similarities, despite the large difference in the chemical functionality.

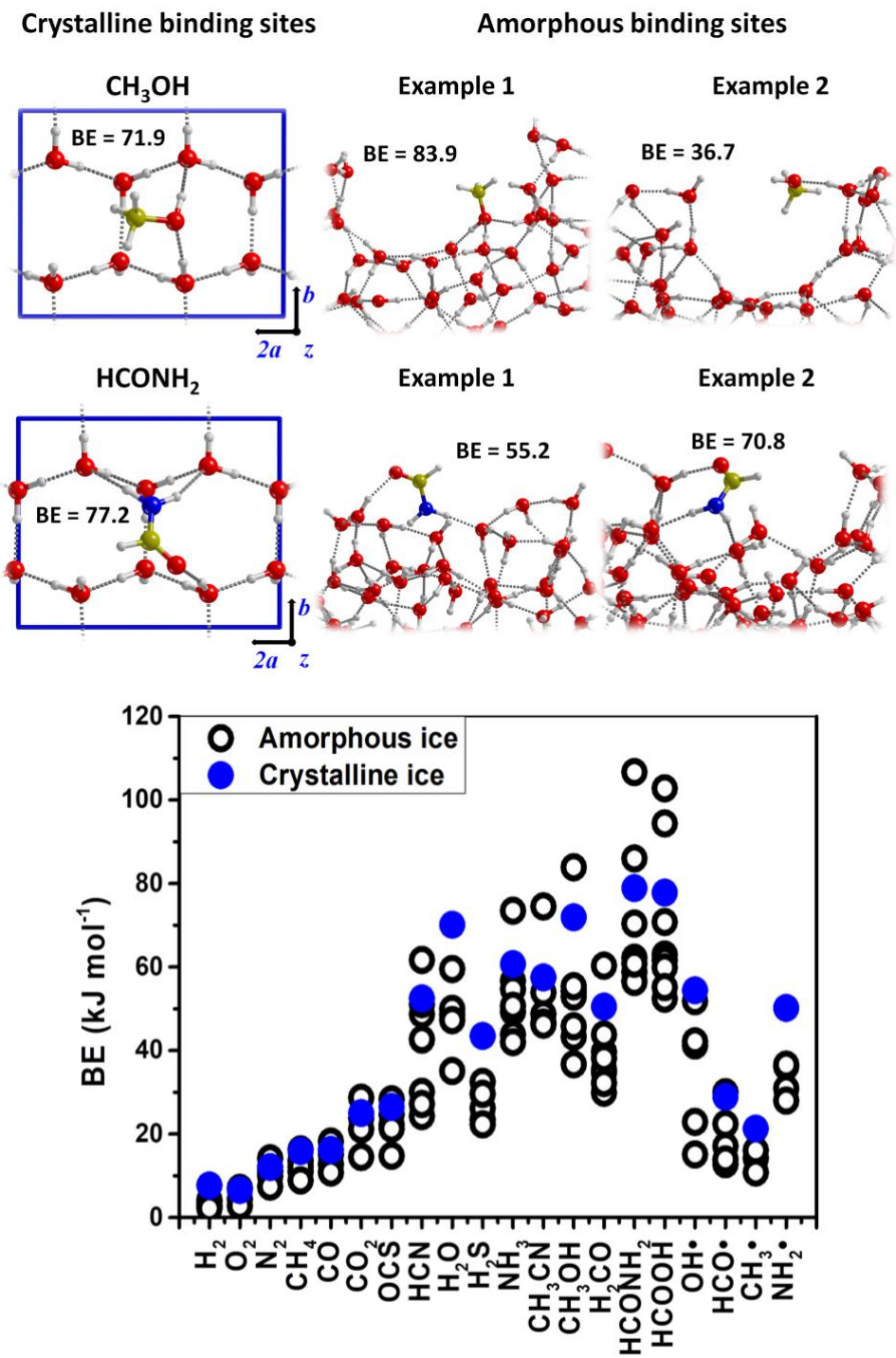

Figure 8 Upper panel: comparison of the final optimized geometries for CH_3OH and $HCONH_2$ (as illustrative examples) on the (010) P-ice crystalline surfaces and on the amorphous slab. BE values are also reported (in kJ mol^{-1}). Lower panel: comparison between adsorbates binding energy for the crystalline and amorphous ice.

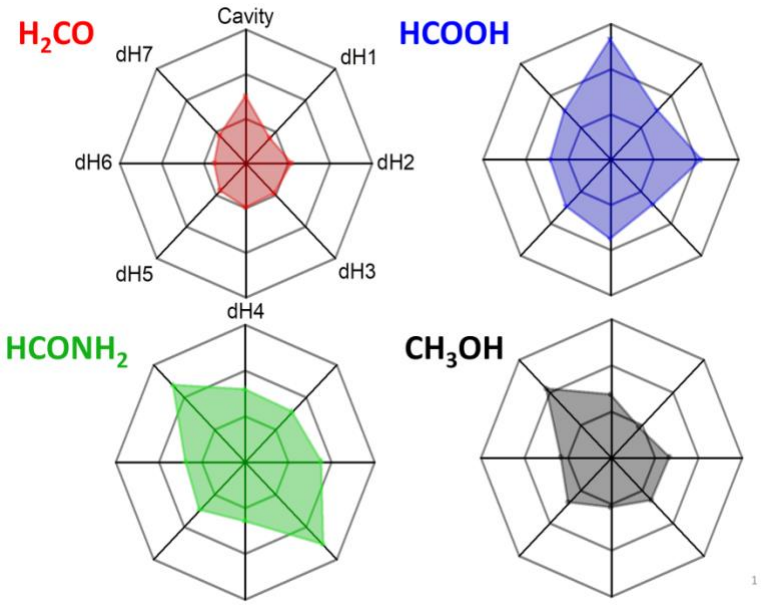

Figure 9 Spider graph of the BE values (in kJ mol^{-1}) calculated on the same adsorption sites of the amorphous slab for the H_2CO (red), CH_3OH (black), $HCONH_2$ (green) and HCOOH (blue) molecules. The BE values scale goes from 0 kJ mol^{-1} (center of the graph) to 120 kJ mol^{-1} (vertices of the polygon).

Table 2 Resume of the data computed on the amorphous ice model and comparison with literature data. Legend: "Min" and "Max": minimum and maximum BE values; "Dev": absolute deviation between our <BE> and that from literature; <Dev>: average deviation for all cases from literature data. Energy data in kJ mol^{-1}.

	Amorphous ice model		BE values from literature				
Species	Min	Max	Das(a)	Wakelam(b)	UMIST(c)	KIDA(d)	Experiment
H_2	2.2	4.2	4.5	6.7	3.6	3.7	
O_2	2.8	7.1	11.2	8.3	8.3	10.0	10(e)
N_2	7.4	14.2	9.7	9.1	6.7	9.1	9.1(e)
CH_4	8.9	16.3	19.3	6.7	9.1	8.0	8(f)
CO	10.8	18.2	10.7	10.8	9.6	10.8	10.8(e)
CO_2	14.5	28.7	19.6	25.8	24.9	21.6	19.1(e)
OCS	14.8	28.3	15.0	17.5	24	20.0	20.2 ± 0.2(g)
HCl	*	*					43(h)
HCN	24.3	61.7	19.6	29.1	22.8	30.8	
H_2O	35.1	59.5	34.6	38.2	40	46.6	
H_2S	22.3	32.5	26.9	24.1	17	22.4	22.8(i)
NH_3	42.0	73.5	42.9	46.6	46	45.7	46(i)
CH_3CN	46.2	74.5	31.5	35.8	38.9	38.9	38.9(i)
CH_3OH	36.7	83.9	37.5	42.4	41	41.6	41.6(i)
H_2CO	29.9	60.3	27.0	42.4	17	37.4	
$HCONH_2$	52.4	102.8	-	52.4	46.2	52.4	
HCOOH	56.4	106.7	29.0	-	41.6	46.3	
OH•	15.1	51.8	26.5	38.2	23.7	38.2	
HCO•	12.8	30.0	15.4	44.1	13.3	20.0	
CH_3•	10.8	16.1	11.0	20.8	9.8	13.3	
NH_2•	28.0	36.6	26.9	37.4	32.9	26.6	

* HCl molecule dissociate. (a) (Das 2018); (b) (Wakelam et al. 2017); (c) (McElroy et al. 2013); (d) (Wakelam et al. 2015); (e) (Minissale et al. 2016); (f) (Raut et al. 2007); (g) (Ward et al. 2012); (h) (Olanrewaju et al. 2011); (i) (Collings et al. 2004)

.

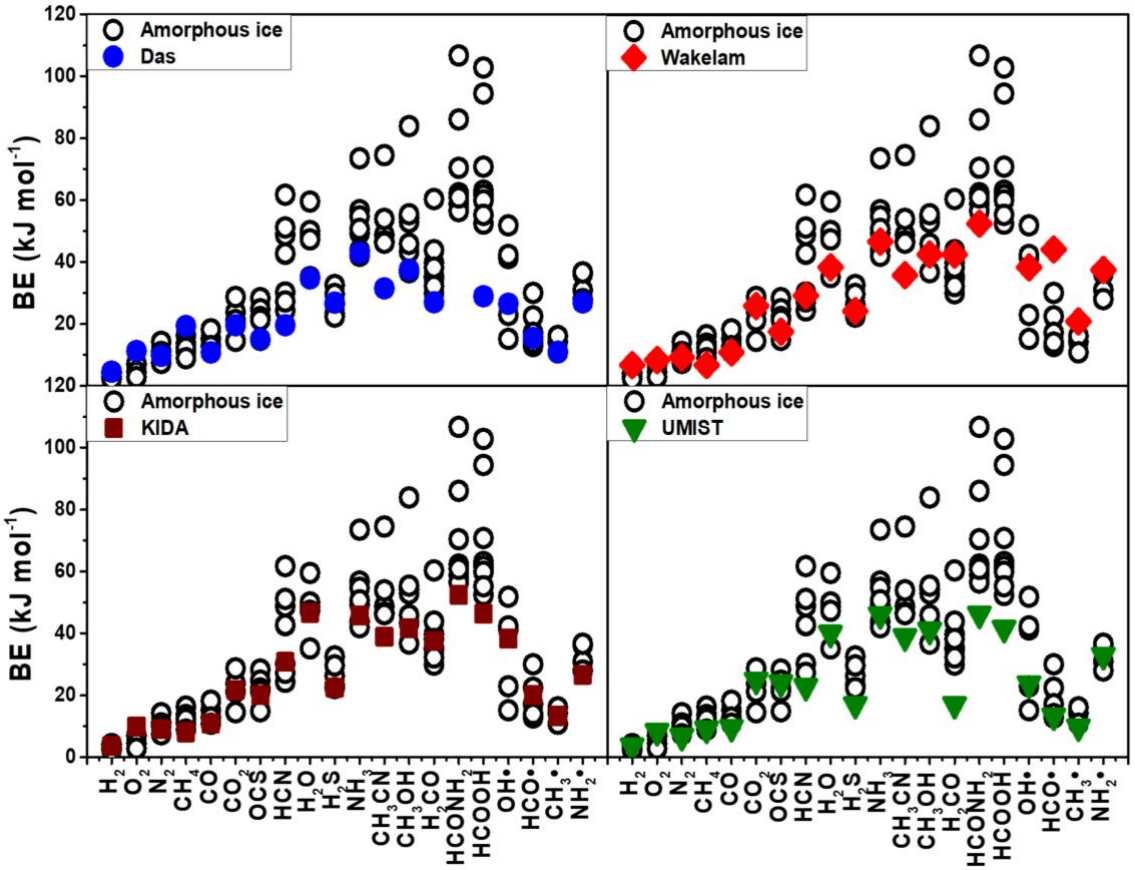

Figure 10 Comparison of the computed BEs for the amorphous ice model with respect to those by Das *et al.*, Wakelam *et al.* and reported in the KIDA and UMIST databases.(Das 2018; McElroy et al. 2013; Wakelam et al. 2017, 2015)

From the comparisons made in **Table 2** it can be inferred that, even with some notable cases with large differences, our BE values are overall, in good agreement with every dataset. It should be noted that our results are very close to the BE values found in literature especially for the weakly bound species (such as H_2, O_2, N_2, CH_4, CO, CO_2, OCS), whereas they tend to overestimate the BEs for larger species which can establish multiple hydrogen bonds with the surface (e.g. CH_3OH, H_2CO, HCOOH, $HCONH_2$). The comparison with the available experimental data (see **Table 2**) revealed a general good agreement with the computed data on the amorphous ice. The most significant deviations are for CH_3OH and CH_3CN with definitely too high computed BE values. There may be many reasons for such discrepancies: i) usually temperature programmed desorption associated with the kinetic equations is adopted in the experiments to arrive to the BE value, while our computed BE should be compared with microcalorimetric data hardly available for adsorption on ice; ii) different energetic cost for restructuring the ice during the adsorption/desorption for model versus experiments; iii) a real ice structure intrinsically different from the adopted model, i.e. less rich in dangling dH bonds responsible for the high computed BE values; iv) deficiencies in the

formulation devoted to take London dispersion contribution into account, with tendency to overestimate its role.

It is important to highlight that limited ice model, like the ones of Wakelam and Das made by few water molecules (up to six molecules), cannot in principle reproduce strong adsorption situations that we have seen on our slab model (see **Figure 8** for examples). The adoption of a more realistic and periodically extended ice models allows to fully consider the hydrogen bond cooperativity which will enhance the strength of the interaction with adsorbates at the terminal dangling hydrogen atoms exposed at the surface. This important effect is entirely missing within a cluster approach for modeling ice, as in the Wakelam model (one water molecule); (Wakelam et al. 2017) and very much so for the small clusters (up to six water molecules) adopted by Das et al. (Das 2018) Furthermore, the present model can be readily adopted to study diffusional barrier for the adsorbates as well as COM formation through ab initio molecular dynamics calculations giving a final coherent picture of the molecular story at ice surfaces.

4 Conclusions

In this work, we present a new computational approach to an important topic in the field of Astrochemistry: the binding energies (BEs) of molecular and radical species on interstellar ice surfaces. We simulated such surfaces by means of two (antipodal) models, in both cases adopting a periodic approach: a crystalline and an amorphous 2D slab models. These two models differ in the electrostatic surface properties, the number of available adsorption sites, the dimension of the repeating unit cell, and the thickness of the slabs. For the crystalline ice case, we selected the (010) surface cut out from the bulk structure of the proton-ordered model known as P-ice.(Casassa et al. 1997) Due to its simplicity, the (010) P-ice surface can be considered as a benchmark case to evaluate the fundamental aspects of the interaction of a solid water matrix with the molecular species at a very reduced computational cost. The amorphous surfaces were generated by merging three well-characterized water clusters of 20 water molecules from previous work.(Shimonishi et al. 2018) The resulting fully optimized bulk structure was subsequently cut out to define the final 2D slab model. On both surface models, we simulated the structure and adsorption energetic features of 17 molecules and 4 radicals, representative of the most abundant species of the dense interstellar medium. While the crystalline surfaces only show very limited variability in the adsorption sites, the amorphous surfaces provide a wide variety of adsorption binding sites, resulting in a distribution of the computed BE. As for the quantum mechanical methods, we relied on density functional theory (DFT), using the B3LYP-D3 and M06-2X widely used functionals combined with a polarized triple-zeta quality basis set to ensure a good representation of both electrostatic and polarization components of the BEs. Both functionals provide a good description of the London dispersion contribution to the BEs.

The analysis of the binding energies computed for the crystalline ice already indicate, besides hydrogen bond interaction, the key role of the London component in dictating the adduct structure at the surface. To further validate the DFT approach, we resorted to an ONIOM-like correction at coupled cluster level, inclusive of single, double and perturbative triple excitations CCSD(T) with a procedure to extrapolate the DFT computed BE values for a basis set envisaging an infinite number of Gaussian functions. Results from this combined procedure confirm the validity of the binding energies computed with the adopted DFT functionals. The computational inexpensive cost associated to the P-ice model was also exploited to check the reliability of a cost-effective HF-3c method adopted to optimize the structures of the same set of adsorbates at the amorphous ice surface sites. This step was needed, as the computational cost of geometry optimization at full DFT for all considered adsorption sites and adsorbates at the amorphous surfaces would have been prohibitively expensive. Indeed, we proved that the binding energies computed at the crystalline ice

surface at DFT//DFT were in very good agreement with that at DFT//HF-3c level allowing to adopt the same procedure for computing the BEs also on the amorphous ice. The BE values at crystalline ice surface are in general higher than those computed at the amorphous ice surfaces. This is largely due to the smaller geometry relaxation cost upon adsorption compared to the amorphous cases, imposed by the tighter network of interactions of the denser crystalline ice over the amorphous ice. The BEs were also compared with literature data, either from computational studies adopting from 1 (Wakelam et al. 2017) to 6 water molecules to mimic the ice surface (Das 2018) and with the available experimental data (see Table 2). In general, the agreement is good considering the different adopted model and computational methodologies.

We feel the present work will have a wide-reaching impact in the Astrochemistry community, as it provides BE values of astrochemically-relevant species on crystalline and amorphous interstellar water ice models, which can be incorporated in astrophysical models aiming to describe the chemico-physical evolution of the interstellar medium.

5 Acknowledgements

SF, LZ and PU acknowledge financial supported from the Italian MIUR (Ministero dell'Istruzione, dell'Università e della Ricerca) and from Scuola Normale Superiore (project PRIN 2015, STARS in the CAOS - Simulation Tools for Astrochemical Reactivity and Spectroscopy in the Cyberinfrastructure for Astrochemical Organic Species, cod. 2015F59J3R). The Italian CINECA consortium are also acknowledged for the provision of supercomputing time for part of this project. AR is indebted to the "Ramón y Cajal" program. MINECO (project CTQ2017-89132-P) and DIUE (project 2017SGR1323) are acknowledged. This project has received funding from the European Union's Horizon 2020 research and innovation programme under the Marie Skłodowska-Curie grant agreement No 811312 for the project "Astro-Chemical Origins" (ACO)."

Authors informations:

Corresponding author

Piero Ugliengo. E-mail: piero.ugliengo@unito.it, telephone: +39 011 670 4596

Other authors

Stefano Ferrero. E-mail: stefano.ferrero899@edu.unito.it

Lorenzo Zamirri. E-mail: lorenzo.zamirri@unito.it

Cecilia Ceccarelli. E-mail: cecilia.ceccarelli@univ-grenoble-alpes.fr

Albert Rimola. E-mail: albert.rimola@uab.cat

ORCID

Stefano Ferrero: 0000-0001-7819-7657

Cecilia Ceccarelli

Piero Ugliengo: 0000-0001-8886-9832

Albert Rimola: 0000-0002-9637-4554

Lorenzo Zamirri: 0000-0003-0219-6150

6 Supporting information

The Supporting Information (SI) file is organized into sections. S1: description of computational details. S2: Images of the geometries of the adsorption of every species with energetic and vibrational data. S3: Plots of the Gaussian distribution built with the BE values found on the amorphous slab model.

Bibliography

Al-Halabi, a., & Van Dishoeck, E. F. 2007, Mon Not R Astron Soc, 382, 1648

Ásgeirsson, V., Jónsson, H., & Wikfeldt, K. T. 2017, J Phys Chem C, 121, 1648

Bartlett, R. J., & Musiał, M. 2007, Rev Mod Phys, 79, 291

Becke, A. D. 1988, J Chem Phys, 88, 2547

Becke, A. D. 1993, J Chem Phys, 98, 1372

Bennett, C. J., & Kaiser, R. I. 2007, Astrophys J, 661, 899

Boogert, A., Gerakines, P., & Whittet, D. 2015, Annu Rev Astron Astrophys, 53, 541

Borden, W. T., Ho, R., Stuyver, T., & Chen, B. 2017, J Am Chem Soc, 139, 9010

Boys, S. F., & Bernardi, F. 1970, Mol Phys, 19, 553

Brown, P. D., & Charnley, S. B. 1990, Mon Not R Astron Soc, 244, 432

Broyden, C. G. 1970, J Inst Math Its Appl, 6, 76

Casassa, S., Ugliengo, P., & Pisani, C. 1997, J Chem Phys, 106, 8030

Chang, Q., Cuppen, H. M., & Herbst, E. 2005, Astron Astrophys, 434, 599

Chang, Q., & Herbst, E. 2012, Astrophys J, 759, 147(15 pp)

Collings, M. P., Anderson, M. A., Chen, R., et al. 2004, Mon Not R Astron Soc, 354, 1133

Cramer, C. J. 2004, Essentials of Computational Chemistry: Theories and Models (Hoboken, New Jersey (USA): Wiley)

Cutini, M., Civalleri, B., Corno, M., et al. 2016a, J Chem Theory Comput, 12, 3340

Cutini, M., Civalleri, B., & Ugliengo, P. 2019, ACS Omega, 4 (American Chemical Society), 1838
Cutini, M., Corno, M., & Ugliengo, P. 2016b, J Chem Theory Comput, 13, 370
Dapprich, S., Komáromi, I., Byun, K. S., Morokuma, K., & Frisch, M. J. 1999, J Mol Struct THEOCHEM, 461, 1
Dartois, E. 2005, in ISO Science Legacy (Dordrecht: Springer), 293
Das, A. et A. 2018, Astrophys J Suppl Ser, 237 (IOP Publishing), 9 (13pp)
Davidson, E. R., & Feller, D. 1986, Chem Rev, 86, 681
Douglas, A. E., & Herzberg, G. 1942, Can J Res, 20, 71
Dovesi, R., Erba, A., Orlando, R., et al. 2018a, Wiley Interdiscip Rev Comput Mol Sci, 8, e1360
Dovesi, R., Saunders, V. R., Roetti, C., et al. 2018b
Draine, B. T. 2003, Annu Rev Astron Astrophys, 41, 241
Dulieu, F., Congiu, E., Noble, J., et al. 2013, Sci Rep, 3, 1338(6 pp)
Dunning Jr, T. H. 1989, J Chem Phys, 90, 1007
Endres, C. P., Schlemmer, S., Schilke, P., Stutzki, J., & Müller, H. S. P. 2016, J Mol Spectrosc, 327, 95
Fayolle, E. C., Balfe, J., Loomis, R., et al. 2015, Astrophys J Lett, 816 (IOP Publishing), L28(6 pp)
Fletcher, R. 1970, Comput J, 13, 317
Goldfarb, D. 1970, Math Comput, 24, 23
Grimme, S., Antony, J., Ehrlich, S., & Krieg, H. 2010, J Chem Phys, 132, 154104 (19 pp)
Grimme, S., Ehrlich, S., & Goerigh, L. 2011, J Comput Chem, 31, 1456
Hasegawa, T. I., & Herbst, E. 1992, Mon Not R Astron Soc, 261, 83
Hasegawa, T. I., Herbst, E., & Leukng, C. M. 1992, Astrophys J Suppl Ser, 82, 167
He, J., Acharyya, K., & Vidali, G. 2016, Astrophys J, 825 (IOP Publishing), 89(10 pp)
He, J., & Vidali, G. 2014, Faraday Discuss, 168 (Royal Society of Chemistry), 517
Herbst, E. 2014, Phys Chem Chem Phys, 16, 3344
Hohenberg, P., & Kohn, W. 1964, Phys Rev, 136, B864
Jansen, H. B., & Ros, P. 1969, Chem Phys Lett, 3, 140
Karssemeijer, L. J., Ioppolo, S., van Hemert, M. C., et al. 2014a, Astrophys J, 781, 16 (15pp)
Karssemeijer, L. J., de Wijs, G. a., & Cuppen, H. M. 2014b, Phys Chem Chem Phys, 16, 15630
Kraus, P., & Frank, I. 2018, J Phys Chem A, 122, 4894
Lee, C., Yang, W., & Parr, R. G. 1988, Phys Rev B, 37, 785
Liu, B., & Mclean, A. D. 1973, J Chem Phys, 59, 4557
McElroy, D., Walsh, C., Markwick, A. J., et al. 2013, Astron Astrophys, 550, A36 (13 pp)
McKellar, A. 1940, Publ Astronmical Soc Pacific, 52, 187

Minissale, M., Dulieu, F., Cazaux, S., & Hocuk, S. 2016, Astron Astrophys, 585, A24
Noble, J. A., Congiu, E., Dulieu, F., & Fraser, H. J. 2012, Mon Not R Astron Soc, 421, 768
Oba, Y., Miyauchi, N., Hidaka, H., et al. 2009, Astrophys J, 701, 464
Oberg, K. I., Boogert, A. C. A., Pontoppidan, K. M., et al. 2008, Astrophys J, 678, 1032
Olanrewaju, B. O., Herring-captain, J., Grieves, G. A., Aleksandrov, A., & Orlando, T. M. 2011, J Phys Chem A, 115, 5936
Pack, J. D., & Monkhorst, H. J. 1977, Phys Rev B, 13, 5188
Papajak, E., Zheng, J., Xu, X., Leverentz, H. R., & Truhlar, D. G. 2011, J Chem Theory Comput, 7, 3027
Pascale, F., Zicovich-Wilson, C. M., López Gejo, F., et al. 2004, J Comput Chem, 25, 888
Penteado, E. M., Walsh, C., & Cuppen, H. M. 2017, Astrophys J, 844, 71 (13 pp)
Pople, J. A., Gill, P. M. W., & Handy, N. C. 1995, Int J Quantum Chem, 56, 303
Raut, U., Famá, M., Teolis, B. D., & Baragiola, R. a. 2007, J Chem Phys, 127
Rimola, A., Civalleri, B., & Ugliengo, P. 2008, Langmuir, 24, 14027−14034
Rimola, A., Taquet, V., Ugliengo, P., Balucani, N., & Ceccarelli, C. 2014, Astron Astrophys, 572, A70 (12 pp)
Schäfer, A., Horn, H., & Ahlrichs, R. 1992, J Chem Phys, 97, 2571
Senevirathne, B., Andersson, S., Dulieu, F., & Nyman, G. 2017, Mol Astrophys, 6 (Elsevier B.V.), 59
Shanno, D. F. 1970, Math Comput, 24, 647
Shimonishi, T., Nakatani, N., Furuya, K., & Hama, T. 2018, Astrophys J, 855 (IOP Publishing), 27 (11pp)
Smith, R. S., May, R. A., & Kay, B. D. 2016, J Phys Chem B, 120, 1979
Sorrell, W. H. 2002, Astrophys J, 555, L129
Sure, R., & Grimme, S. 2013, J Comput Chem, 34, 1672
Swings, P., & Rosenfeld, L. 1937, Astrophys J, 86, 483
Taquet, V., Ceccarelli, C., & Kahane, C. 2011, Astron Astrophys, 538, A42(19 pp)
Tasker, P. W. 1979, J Phys C Solid State Phys, 12, 4977
Tatewaki, H., & Huzinaga, S. 1980, J Comput Chem, 1, 205
Tentscher, P. R., & Arey, J. S. 2013, J Chem Theory Comput, 9, 1568
Tosoni, S., Pascale, F., Ugliengo, P., et al. 2005, Mol Phys, 103, 2549−2558
Ugliengo, P., & Damin, A. 2002, Chem Phys Lett, 366, 683
Vasyunin, A. I., & Herbst, E. 2013, Astrophys J, 762, 86(21 pp)
Wakelam, V., Loison, J. C., Herbst, E., et al. 2015, Astrophys Journal, Suppl Ser, 217 (IOP

Publishing), 20
Wakelam, V., Loison, J., Mereau, R., Ruaud, M., & Bordeaux, D. 2017, Mol Astrophys, 6, 22
Ward, M. D., Hogg, I. A., & Price, S. D. 2012, 1269, 1264
Watanabe, N., & Kouchi, A. 2008, Prog Surf Sci, 83, 439
Zamirri, L., Casassa, S., Rimola, A., et al. 2018, Mon Not R Astron Soc, 480 (Oxford University Press), 1427
Zamirri, L., Corno, M., Rimola, A., & Ugliengo, P. 2017, ACS Earth Sp Chem, 1, 384
Zamirri, L., Pantaleone, S., & Ugliengo, P. 2019a, J Chem Phys, 150, 064702 (9 pp)
Zamirri, L., Ugliengo, P., Ceccarelli, C., & Rimola, A. 2019b, ACS Earth Sp Chem, 3 (American Chemical Society), 1499
Zicovich-Wilson, C. M., Pascale, F., Roetti, C., et al. 2004, J Comput Chem, 25, 1873